Journal of Great Lakes Research 40 Supplement 3 (2014) 151–161

Contents lists available at ScienceDirect

Journal of Great Lakes Research

journal homepage: www.elsevier.com/locate/jglr

Modeling Lake Erie's hypoxia response to nutrient loads and physical variability

Daniel K. Rucinski [a,b,*], Joseph V. DePinto [a], Donald Scavia [c], Dmitry Beletsky [d]

[a] LimnoTech, 501 Avis Drive, Ann Arbor, MI 48108, USA
[b] School of Natural Resources and Environment, University of Michigan, 440 Church St., Ann Arbor, MI 48109, USA
[c] Graham Sustainability Institute, University of Michigan, School of Natural Resources and Environment, 625 East Liberty Road, Ann Arbor, MI 48193, USA
[d] Cooperative Institute for Limnology and Ecosystems Research, School of Natural Resources and Environment, University of Michigan, 440 Church St., Ann Arbor, MI 48109, USA

ARTICLE INFO

Article history:
Received 4 September 2013
Accepted 16 December 2013
Available online 4 March 2014

Communicated by Ram Yerubandi

Keywords:
Lake Erie
Hypoxia
Loading
Eutrophication

ABSTRACT

A 1-dimensional, linked hydrodynamic and eutrophication model was developed and calibrated with 19 years of observations (1987–2005) for the summer stratification period in the central basin of Lake Erie, corroborated by comparison with observed process rates and areal hypoxic extents, and confirmed with observations from the 1960s and 1970s. The model effectively captures observations of both vertical and temporal trends in dissolved oxygen, as well as temporal trends in chlorophyll-a, phosphorus, zooplankton biomass, and several key processes. The model was used to develop a relationship between external phosphorus load and hypolimnion oxygen conditions, and then to establish load–response envelopes that account for inter-annual variability in physical conditions driven by variation in meteorological drivers. The curves provide a valuable tool for reassessing phosphorus loading targets with respect to reducing hypoxia in Lake Erie.

Introduction

Lake Erie experienced cultural eutrophication (Beeton, 1963), recovery in response to load reductions (DePinto et al., 1986), and a recent return to eutrophic conditions of the past (Bridgeman et al., 2013; Burns et al., 2005; Zhou et al., 2013). Among symptoms of eutrophication, hypoxia (dissolved oxygen concentration below 2 $mg \cdot L^{-1}$) has been a key indicator for Lake Erie's central basin (El-Shaarawi, 1987; Rosa and Burns, 1987) and excess phosphorus (P) loading from point and agricultural non-point sources (Dolan, 1993; Dolan and Chapra, 2012) has been the key driver in both its growth and recovery phases.

In response to concern about the consequences of eutrophication in the 1960 and 1970s, the governments of the U.S. and Canada, largely through the auspices of the Great Lakes Water Quality Agreement (GLWQA, 1978), implemented a program of P load reduction that was globally unprecedented (DePinto et al., 1986). A combination of point and non-point phosphorus load reductions achieved the target load of 11,000 metric tons per year, and the response of the lake was rapid, profound, and close to that predicted by models. However, despite this apparent success at reducing central basin hypoxia, eutrophication reemerged in the mid-1990s and is now approaching extents of the early decades (Zhou et al., 2013).

Among the several natural and anthropogenic factors potentially responsible for altering hypoxic conditions, changes in climate and hydrology (Blumberg and Di Toro, 1990; Diaz, 2001) and changes in phosphorus loading are key, and thus the subject of this analysis. To perform this analysis, we employed a 1-dimensional linked hydrodynamic-eutrophication model for the Central Basin of Lake Erie. This model offers three key innovations: 1) testing the system response variability over 19 years of observed conditions; 2) employing a novel relationship for estimating SOD under future loads; and 3) for the first time providing simulations and forecasts for hypoxic area (as opposed to DO concentration) under a range of nutrient loads. Hypoxic area is a key management target, and this is the first model to provide those projections. While the potential role of the invasive benthic filter feeders (e.g., zebra and quagga mussels; Woynarovich, 1961), the potential contribution of winter diatom growth to summer oxygen demand (Twiss et al., 2013), and the impact of circulation patterns (Beletsky et al., 2013; Rao et al., 2008) cannot be discounted, they are not the focus of this paper.

Modeling approach

Several linked or coupled hydrodynamic-eutrophication models have been developed for Lake Erie. The spatial sophistication of these works has varied from a 1D approach as demonstrated here, to 2D (Zhang et al., 2008) and 3D domains (Di Toro and Connolly, 1980; Di Toro et al., 1987; Leon et al., 2011). The complexity of the biological portion of the models has varied greatly, ranging from simple statistical relationships

* Corresponding author at: LimnoTech, 501 Avis Drive, Ann Arbor, MI 48108, USA.
E-mail address: drucinski@limno.com (D.K. Rucinski).

http://dx.doi.org/10.1016/j.jglr.2014.02.003
0380-1330/

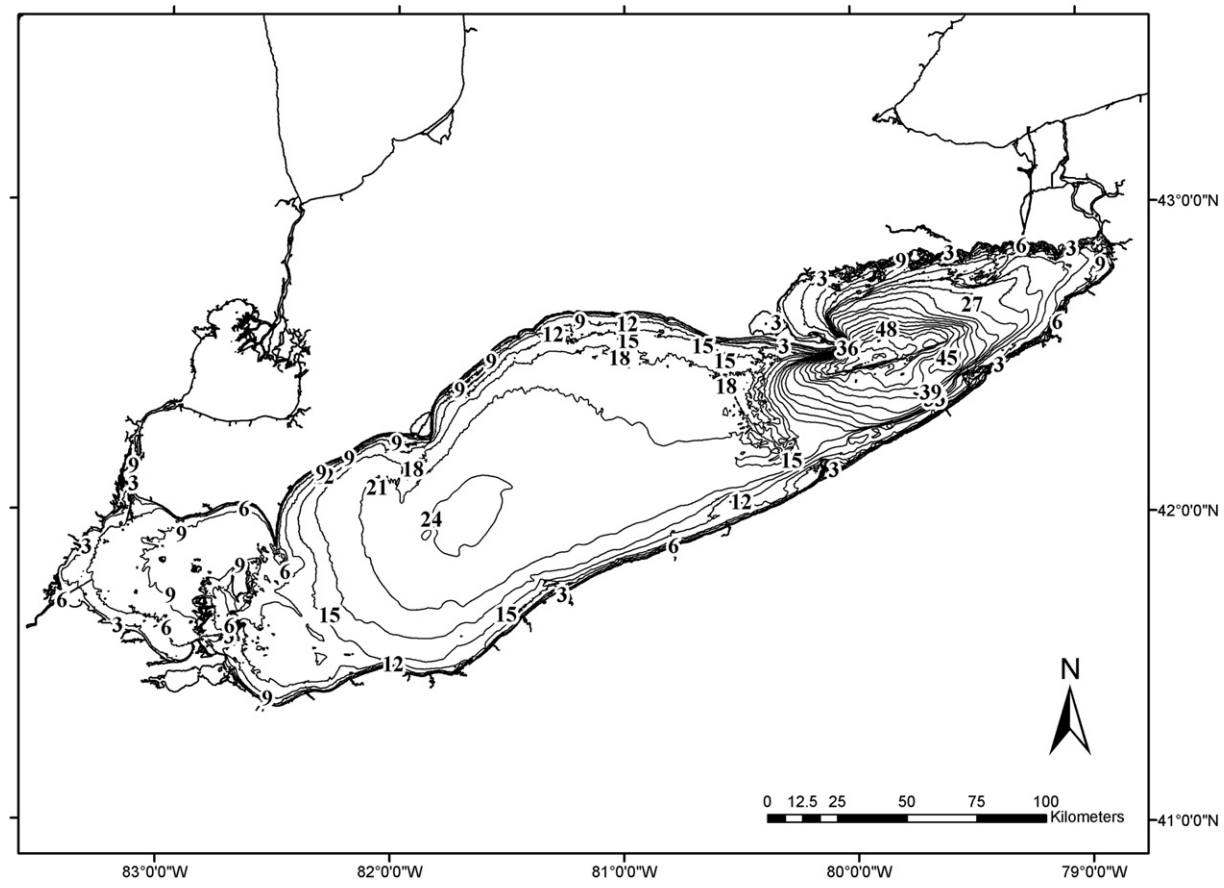

Fig. 1. Morphometry of Lake Erie.

(Burns et al., 2005; Rosa and Burns, 1987; Rucinski et al., 2010) to models using dozens of state variables across multiple environmental media (Leon et al., 2011). All of these approaches have merit for investigating specific forcings of hypoxia in Lake Erie, such as near shore nutrient cycling, or cross lake nutrient transport. However, they are generally limited in their ability to provide forecast management scenarios, either due to exorbitant computation time or lack of input data at the required spatial and temporal scales. Our 1D approach allows for quick simulation of several dozen hypothetical scenarios related to reductions in nutrient loads, inter-annual variability in physical drivers, and long-term change in sediment oxygen demand (SOD) associated with such loads.

Rucinski et al. (2010) demonstrated, with a 1D hydrodynamic model linked to a very simple oxygen demand model that, after accounting for inter-annual variability in temperature and mixing regimes driven by meteorological conditions, there remains significant inter-annual variability and trends in the water column oxygen demand. This oxygen demand is driven by in situ decomposition of autochthonous production of organic matter, which is in turn driven by the availability of

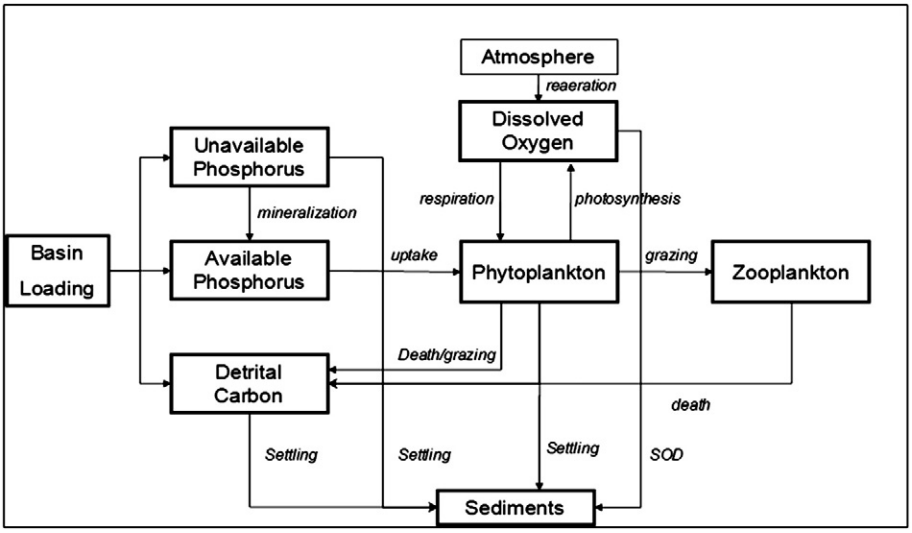

Fig. 2. Conceptual diagram of simple eutrophication model.

phosphorus, the limiting nutrient. To explore those relationships, we developed a eutrophication model, driven by 19 years (1987–2005) of observed nutrient loads and meteorology, to simulate the phosphorus-driven production of organic matter and the contribution of its decay to the evolution of hypolimnion hypoxia in the Central Basin. The model was calibrated to water quality observations from the same 19-year period and compared to observed process rates where available. It should also be noted that this period includes both the decline and the re-emergence of hypoxia through the 1990s (Zhou et al., 2013).

Our one-dimensional hydrodynamic model, representing the offshore waters of the central basin (maximum 24 m in depth, Fig. 1), provided the thermal structure and associated vertical mixing input to the eutrophication model. Both models operate on the same spatial scale of 48 half-meter thick layers. The 1-D physical model is based on the Princeton Ocean Model (Blumberg and Mellor, 1987) and was applied previously for Lake Michigan (Chen et al., 2002) and Lake Erie (Rucinski et al., 2010). It uses the Mellor–Yamada turbulence closure scheme to parameterize vertical mixing (Mellor and Yamada, 1982), and is driven by hourly meteorological observations from the Cleveland, Ohio airport with overland–overlake correction described in Beletsky and Schwab (2001).

Table 1
Equations and terminology of the eutrophication model.

Phytoplankton

$\frac{\partial Pc_n}{\partial t} = Pg_n - \mathrm{Pr}_n - Pvs_n + Pvs2_n + Diff_u + Diff_L - Out$

Where: Pc_n = phytoplankton carbon in model segment n
Pg_n = phytoplankton growth in model segment n
Pr_n = phytoplankton respiration in model segment n
Pvs_n = settling across the interface between segment n_{+1} and segment n
$Pvs2_n$ = settling across the interface between segment n_{-1} and segment n
$Diff_u$ = Turbulent dispersion across the interface between segment n_{-1} and segment n
$Diff_L$ = Turbulent dispersion across the interface between segment n_{+1} and segment n
Out = advection from model segment n to eastern basin

Zooplankton

$\frac{\partial Zoo_n}{\partial t} = Zg_n - Zd_n - Zr_n - Out$

Where: Zoo_n = zooplankton carbon in model segment n
Zg_n = zooplankton growth in model segment n
Zr_n = zooplankton respiration in model segment n
Zd_n = zooplankton death in model segment n

Unavailable phosphorus

$\frac{\partial UP_n}{\partial t} = Wup_n - Pvs_n + Pvs2_n + Diff_u + Diff_L + UP_{rec,n} - MinP_n - Out$

Where: UP_n = unavailable phosphorus in model segment n
Wup_n = unavailable phosphorus load in model segment n
$UP_{rec,n}$ = recycled unavailable phosphorus via zooplankton grazing and phytoplankton and zooplankton death in segment n
$MinP_n$ = mineralization of unavailable to available P in segment n

Available phosphorus

$\frac{\partial AP_n}{\partial t} = Wap_n - Pvs_n + Pvs2_n + Diff_u + Diff_L + AP_{rec,n} + MinP_n - Out$

Where: UP_n = available phosphorus in model segment n
Wap_n = available phosphorus load in model segment n
$UP_{rec,n}$ = recycled available phosphorus via zooplankton grazing and phytoplankton and zooplankton death in segment n
$MinP_n$ = mineralization of unavailable to available P in segment n

Organic carbon

$\frac{\partial OC_n}{\partial t} = Woc_n - Pvs_n + Pvs2_n + Diff_u + Diff_L - Oxid_n + \mathrm{Pr}_n + Zd_n + Zr_n - Out$

Where: OC_n = organic carbon in model segment n
Woc_n = organic carbon load in model segment n
$Oxid_n$ = oxidation of organic carbon in segment n

Dissolved oxygen

$\frac{\partial DO_n}{\partial t} = \mathrm{Rear}_n + Pg_n - \mathrm{Pr}_n + Diff_u + Diff_L - Oxid_n - SOD - Out$

Where: DO_n = dissolved oxygen in model segment n
Rear = re-aeration at the surface
SOD = sediment oxygen demand in the bottom layer

Calibration and confirmation of the hydrodynamic model are fully described in Rucinski et al. (2010). Briefly, calibration was accomplished using temperature data from 1994, representative of central basin open water conditions, and confirmed with data collected in 2005. Maximum model error (represented as RMSE) varied with depth, and found to be 1.9 °C and 3.4 °C for 1994 and 2005, respectively. Both years exhibited maximum errors near thermocline depth. While some model errors can be attributed to either inaccuracies in forcing functions or model physics (e.g. vertical mixing parameterization), others can be attributed to 3D effects that are not represented in a 1D model, such as internal wave propagation, horizontal and vertical advection and diffusion. In particular, mid-lake thermocline conditions can be impacted by vertical velocities (upwelling or downwelling) generated by wind stress curl (Beletsky et al., 2012).

The hydrodynamic and eutrophication models are linked by first simulating the thermal structure of the model domain, and then passing the hourly outputs from the hydrodynamic model (i.e., temperature and vertical mixing coefficients) to the eutrophication model. Both models are initialized annually because the ice cover period was not represented in this version of the Princeton Ocean Model. The date of initiation varies annually, based on the earliest ice-free temperature observations; typically between mid-March and mid-April. Eutrophication state variables are similarly initialized for each year, using the earliest cruise sample concentration, generally occurring in March or April. Therefore, each year was simulated separately, as opposed to a continuous 19-year simulation.

The eutrophication model incorporates external phosphorus and carbon loading, internal phosphorus and carbon cycling, algal growth, death, and sinking, zooplankton grazing, oxygen consumption and production, and sediment interactions (Fig. 2). Stoichiometry among the state variables follows Redfield (1934). Algal growth rate is based

Table 2
Parameters, values and units used in the 1-D model.

Variable group	Parameter	Value	Units	Literature range
Phosphorus	Phosphorus half-saturation	0.001	$mg \cdot L^{-1}$	0.001[a]
Phosphorus	Phosphorus:carbon ratio	0.01		0.01–0.05[a]
Phosphorus	***Mineralization rate***	0.03	1/day	0.03[b]
Phosphorus	Temperature coefficient	1.08		1.08[a,b]
Phosphorus	***Phosphorus settling rate***	0.06	m/day	
Light	Physical light extinction	0.3	1/m	
Light	Self shading	0.3	(L/mgC)/m	0.2–0.7[a]
Light	Photo period	0.5	day	0.3–0.7[a]
Light	Saturating light intensity	350	ly/day	200–500[a]
Phytoplankton	***Max growth rate***	2.7	1/day	2.0–3.0[a]
Phytoplankton	Temperature coefficient	1.08		1.06–1.08[a]
Phytoplankton	Optimal growth temp	22	C	
Phytoplankton	Respiration rate	0.1	1/day	0.075–0.125[a]
Phytoplankton	Temperature coefficient	1.08		1.05–1.08[a]
Phytoplankton	Settling rate	0.05	m/day	0.01–0.1[a]
Phytoplankton	Temperature coefficient	1.028		1.02–1.028[a]
Phytoplankton	Carbon:chlorophyll ratio	40		20–50[a]
Zooplankton	***Grazing rate***	2	(L/mgC)/day	
Zooplankton	Respiration rate	0.03	1/day	
Zooplankton	Temperature coefficient	1.04		
Zooplankton	Grazing efficiency	0.6		0.6[b]
Zooplankton	***Death rate***	0.05	1/day	
Zooplankton	Temperature coefficient	1.08		1.08[b]
Oxygen	Surface transfer coeff.	0.2	m/d	
Oxygen	Temperature coefficient	1.024		1.02–1.028[a]
Oxygen	Oxygen:carbon ratio	2.67		2.67[a,b]
Oxygen	Oxygen:phosphorus ratio	267		
Oxygen	SOD	0.75	g/m2/d	0.2–4.0[a]
Carbon	Oxygen half saturation	0.4	mgO_2/L	0.5[a]
Carbon	***Oxidation rate***	0.2	1/day	0.1[b]
Carbon	Temperature coefficient	1.08		1.08[a]
Carbon	***Detritus settling rate***	0.05	m/d	

[a] Wool et al., 2002.
[b] Di Toro and Connolly, 1980.

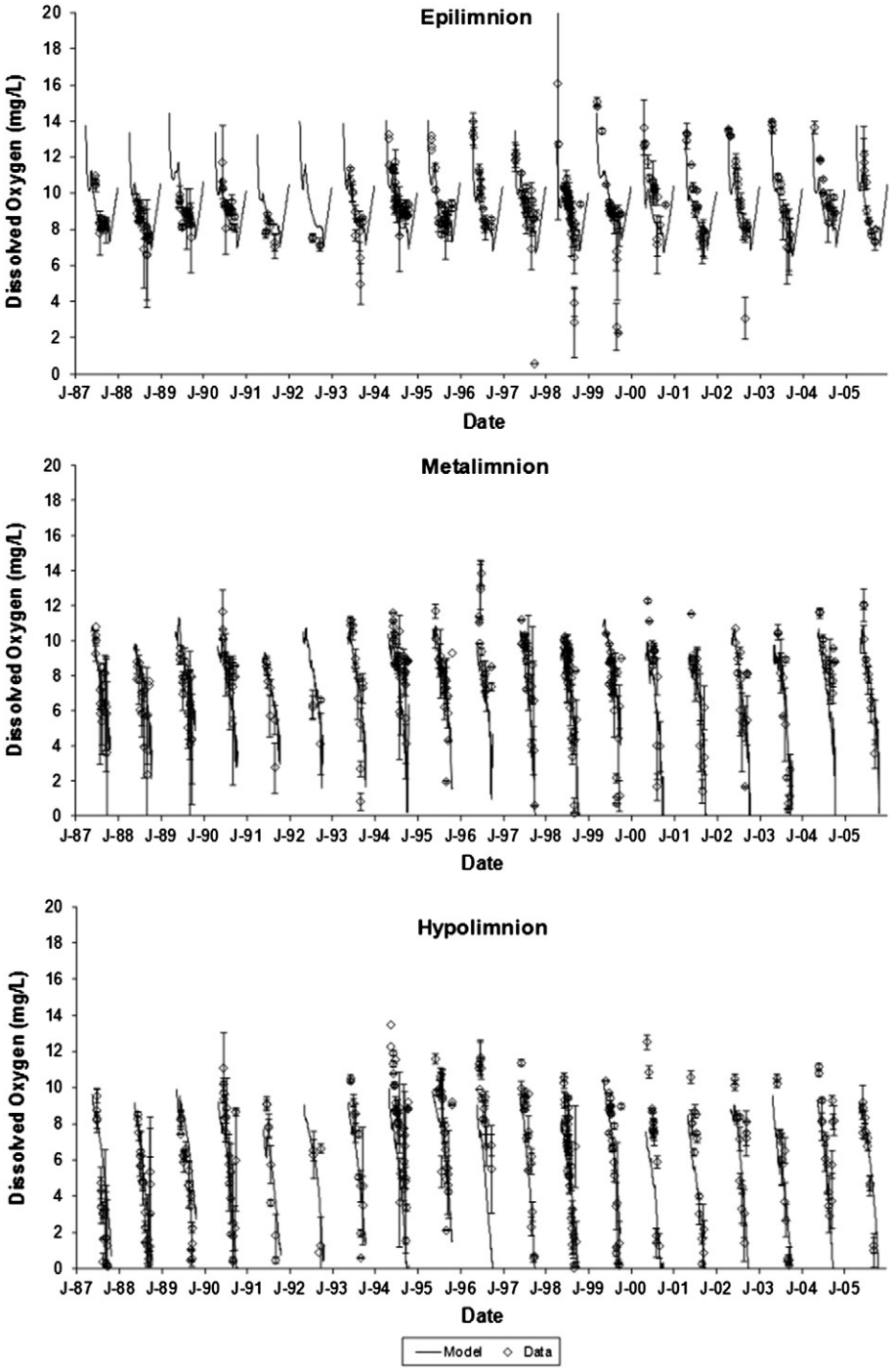

Fig. 3. Comparison of model (line) and data (open diamonds) for mixed-layer averages of dissolved oxygen 1987–2005.

on uptake of available phosphorus following the Michaelis–Menten relationship, light limitation as a function of a constant extinction coefficient with self-shading from algal biomass, and water temperature. Algal photosynthesis and respiration are temperature-dependent 1st order rates, as are settling terms and mineralization of unavailable to available phosphorus. For calibration, sediment oxygen demand (SOD) is a 0th order areal flux (see below regarding SOD estimates for future scenarios). These differential equations (Table 1) are solved using a Euler integration scheme, and, with details on the kinetic processes outlined in Supporting Information Table S1.

Observations

Long-term (1987–2005) observations of dissolved oxygen (DO), total phosphorus (TP), dissolved reactive phosphorus (DRP), and chlorophyll-a (CHL) were compiled from several stations in the central basin of Lake Erie. Zooplankton data were far less abundant, with only the 2005 data used in this analysis. Data were obtained from multiple sources, including EPA's online database (GLENDA), EPA's Great Lakes National Program Office (GLNPO), Environment Canada's Water Science & Technology Branch (ECWSTB), and the International Field

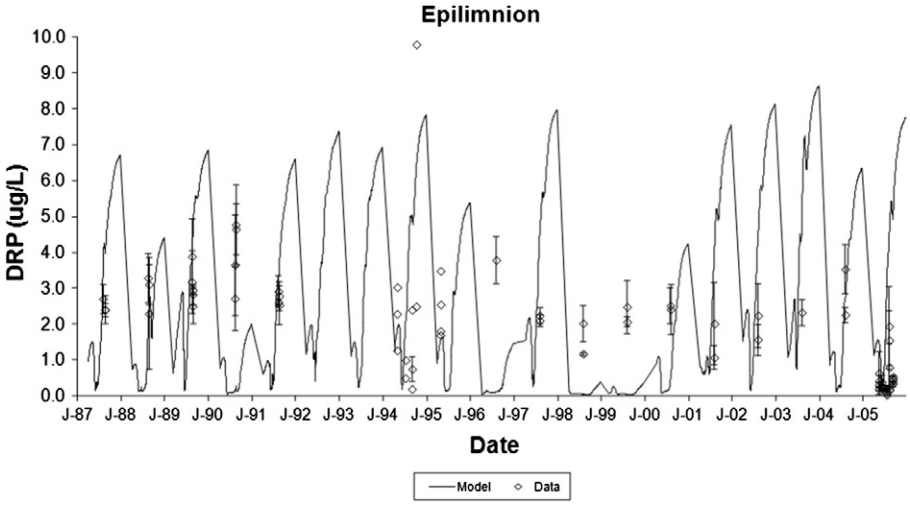

Fig. 4. Comparison of model (line) and data (open diamonds) for epilimnion mixed-layer average of dissolved reactive phosphorus 1987–2005.

Years on Lake Erie Program (IFYLE, 2006) for central basin stations with an average depth of 20 m.

TP loads are from Dolan (1993) and Dolan and McGunagle (2005), and DRP loads (available P in the model) are from Richards (2006) and Richards and Baker (2002). Significant manipulation was required to convert these data into model inputs. First, loads to the western basin were routed to the central basin after accounting for a constant net apparent settling loss of 10 $m \cdot yr^{-1}$ based on an estimate of basin specific net apparent settling rates for phosphorus via a post-audit of The Great Lakes Total Phosphorus Model (Lesht et al., 1991).

We then apportioned these TP loads, as well as those entering the central basin, into available and unavailable portions on a daily basis in the following manner. Dolan (1993) and Dolan and McGunagle (2005) provide western and central basin annual water year (Oct–Sept) loads. Richards (2006) and Richards and Baker (2002) provide daily loads of both TP and DRP for the Maumee and Raisin rivers that flow into the western basin and the Sandusky, Vermillion, Cuyahoga, and Grand (Ohio) rivers that flow into the central basin. To apportion the TP loads, we summed the daily loads into water year totals and established a ratio of this subset of daily-derived annual loads to the total basin loads. We then used this ratio to decompose the Dolan-computed total basin loads to daily loads by applying the ratio to the daily load time-series Richards (2006) and Richards and Baker (2002). For example, if the total measured water-year Maumee plus Raisin TP loads was 2500 metric tons, and the total western basin load from all tributaries in that water year was 7500 metric tons, a scaling factor of 3.0 would be applied to the daily Maumee plus Raisin loads to provide daily total western basin loads.

A slightly modified approach was used to estimate daily DRP loads. We applied the daily DRP:TP ratio from Richards (2006) and Richards and Baker (2002) to the daily TP loads derived after applying the net apparent settling loss, as described above. Finally, the DRP load from the Detroit River was based on the estimates by Dolan (1993) and an average DRP:TP ratio from Richards (2006). Due to lack of available daily Detroit River loading estimates over the study period, we assumed that this portion of the load was constant. Particulate P load was estimated as the difference between TP and DRP. Note that the eastern basin loading is ignored in this analysis.

The base light extinction coefficient (0.3 m^{-1}) was estimated from extensive data on photosynthetic active radiation at varying depths in the central basin (GLNPO). Measured sediment oxygen demand (SOD) has not varied significantly over the analysis period, so for model calibration and testing we used an average value of 0.75 $gO_2 \cdot m^{-2} \cdot day^{-1}$ (Matisoff and Neeson, 2005; Schloesser et al., 2005; Snodgrass, 1987;

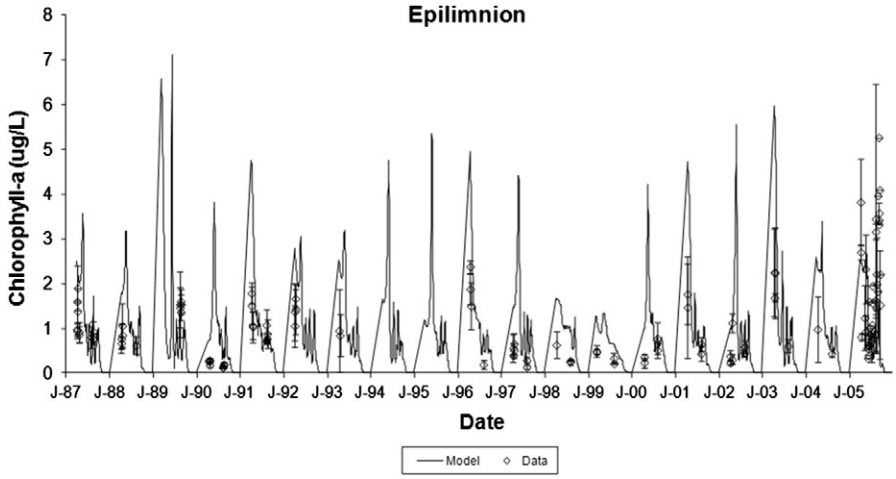

Fig. 5. Comparison of model (line) and data (open diamonds) for epilimnion mixed-layer average of chlorophyll-a 1987–2005.

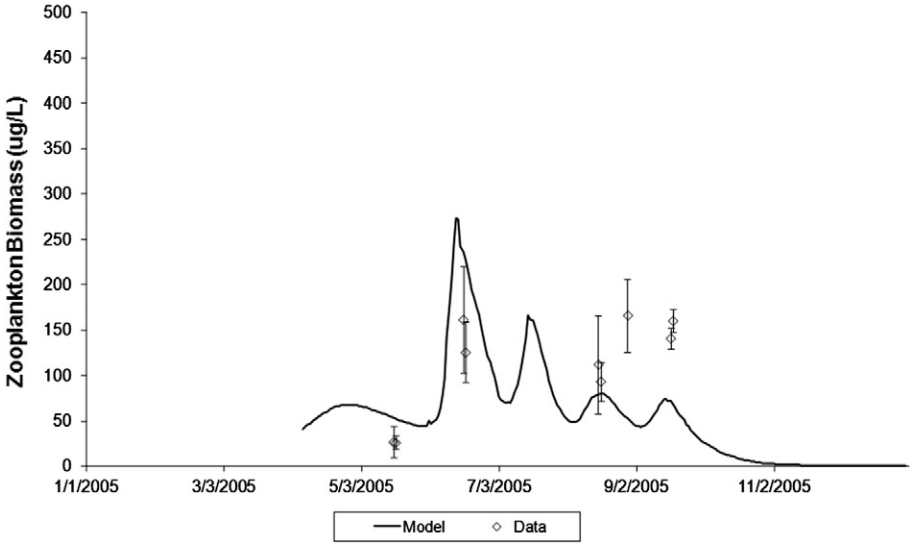

Fig. 6. Comparison of model (line) and data (open diamonds) for epilimnion mixed-layer average of zooplankton 2005.

Snodgrass and Fay, 1987), corrected for temperature deviations from 20 °C. Other rate coefficients were adjusted within the bounds of literature values during calibration (Table 2).

Model parameterization and evaluation

Model performance was assessed by comparing model output to state variable observations with the same parameter values over the entire 19 year data set (1987–2005). Model coefficients were determined via an iterative calibration/corroboration process, focusing on DO and CHL observations, and to a lesser extent on DRP and zooplankton biomass because data for those constituents were less available. While particular emphasis was placed on calibrating to the 1994 and 2005 observations because those years had the most observations, additional modest adjustments were used in the corroboration with other years in the 1987–2005 dataset. Table 2 lists the coefficient values, as well as calculated rates based on data (SOD, light extinction). Parameters in bold italics are the ones that were adjusted. While data were collected much less frequently in some years, we believe that the length of the record serves as an adequate corroboration dataset.

For comparisons, both model output and observations were aggregated into mixed layer averages, representing the epilimnion, metalimnion, and hypolimnion based on the temperature profiles from the hydrodynamic model. The metalimnion was estimated as the zone where the temperature gradient was at least 1 °C/m (Wetzel, 2001). Because stratification in the hydrodynamic model varies, the depth of the bottom of the metalimnion (i.e., top of the hypolimnion) changes both seasonally and annually as a consequence of meteorological inputs.

Results

The model captures the temporal trends in DO, CHL, and zooplankton (where data are available). Results for DO (Fig. 3), DRP (Fig. 4), and CHL (Fig. 5) show best correspondence in years where the calibration was not only most focused (1994, 2005) but also quite well in the full corroboration data set. The vertical trends in DO are captured well. Comparison with vertically averaged zooplankton (Fig. 6) was only possible for 2005. The temporal trends in DRP are difficult to delineate because those data are only available for the late summer in most

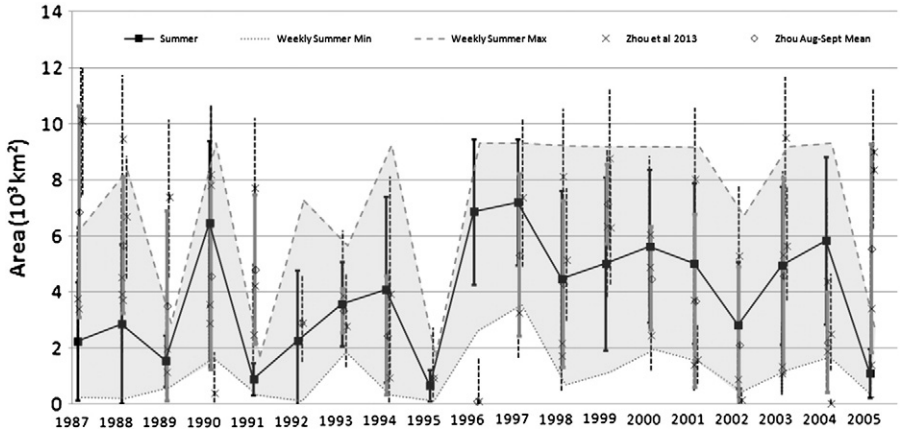

Fig. 7. Cross symbols with dashed error bars are 95% confidence intervals for individual cruises (Zhou et al., 2013). The shaded region represents model output 7-day minimum and maximum for August–September. Open diamonds and gray error bars are monthly means and standard deviation of the individual cruise estimates. Dark black line and bars represent model Aug–Sept means and standard deviation.

Table 3
Recent published primary production rates in Lake Erie for comparison with model estimates.

Reference	Minimum production ($mgC \cdot m^{-3} \cdot day^{-1}$)	Maximum production ($mgC \cdot m^{-3} \cdot day^{-1}$)
Ostrom et al. (2005a)	11.5	395.5
Ostrom et al. (2005b)	76.8	230.4
Depew et al. (2006)	37.0	85.1
Smith et al. (2005)	50.2	81.9
Model estimates	18.7	92.7

years. However, as expected the values reach very low concentrations coinciding with increased phytoplankton and zooplankton abundance.

As another corroboration test, we used model output from the layers located within the daily evolving hypolimnion, and a relationship between bottom water dissolved DO and hypoxic area ($A = 9.3\exp(-DO^2 / 7.09)$) developed by Zhou et al. (2013) to compare modeled areal extent to those estimated from a geostatistical analysis of the observations (Zhou et al., 2013). It is important to note that hypoxic area derived from geostatistical analysis of observations from individual cruises (Zhou et al., 2013) varies considerably within a year, even when cruises were only a few weeks apart (Fig. 7). Yet, the model captures that intra-annual variability, expressed as the minimum and maximum 7-day averages for each summer, and a comparison between modeled and observed summer hypoxic area, averaged over the timeframe of the observations in each year, shows that the model also captures the inter-annual dynamics of this key management-focused metric.

While the model is relatively simple, containing only six state variables, there are over thirty parameters that can be adjusted during calibration. The vast majority of these parameter values are within ranges used in similar models of large lakes, from the literature, and from the EPA model guidelines (Table 2). However, in such under-determined models (Anderson, 2005; Friedrichs et al., 2006), it is possible to match state variable observations with more than one set of rate coefficients, such that over-estimation of one rate process is compensated by under-estimation of another. For this reason and to further confirm model performance, we also compared the calibrated model results to sedimentation, primary production, and oxygen depletion rates. The June–September mean primary production rates calculated by the model (18.7–92.7 $mgC \cdot m^{-3} \cdot day^{-1}$) are within the range of values measured during the growing season (Table 3). There are fewer published measurements of sedimentation rates in Lake Erie, particularly in recent decades. However, the model average of 1.59 g(dw) m^{-2} day^{-1} is consistent within the 0.2–71.2 g(dw) m^{-2} day^{-1} range measured in Lake Erie by Charlton and Lean (1987) and the 1.47–2.2 g(dw) m^{-2} day^{-1} range measured in offshore Lake Ontario by Rosa (1985). Modeled hypolimnetic dissolved oxygen depletion rates are also comparable to those estimated by the much simpler models (Rucinski et al., 2010), by regression of hypolimnetic averaged concentrations (Fig. 8), and by Burns et al. (2005) and Rosa and Burns (1987).

Overall, the calibration, corroboration, and confirmation tests outlined above (as well as the additional tests to data outside the calibration set described below) provide sufficient confidence in the model's ability to reproduce hypoxia dynamics on seasonal and inter-annual scales.

In an earlier analysis that aggregated all oxygen consumption into water column and sediment demands, Rucinski et al. (2010) found that SOD represented on average 63% of the total hypolimnetic oxygen demand. In the present model, SOD also represents a substantial fraction of the overall demand. For example, in a simple model test of removing all external phosphorus load, it still required a 67% reduction of SOD to eliminate hypoxia.

Because SOD is dependent upon settled organic matter, primarily from phytoplankton production driven by nutrient loads, it is logical to assume that reduced loads would eventually lead to reduced SOD (Smith and Matisoff (2008). So, we needed estimates of SOD changes in response to projected changes in phosphorus loads. To account for this, we relied first on a relationship developed by Borsuk et al. (2001) between SOD and carbon deposition:

$$SOD = a\left(\frac{L_c}{1 + kL_c h}\right)^b$$

where L_c is deposited organic carbon, h is the thickness of the hypolimnion, and a, b, and k are the model coefficients. Although their study focused mostly on large estuaries, we were able to calculate values for a, b, and k via a least-squares regression such that the equation reproduced the average observed SOD for rates of organic carbon deposition simulated by the eutrophication model across the range of loads from the 19-year data set (Fig. 9). This provides a reasonable representation of the relationship between carbon sedimentation and SOD. However, to adjust SOD in our load-reduction scenarios, we need to know how SOD would vary with nutrient load. To address this, we ran the current model over a wide range of loads to generate a relationship

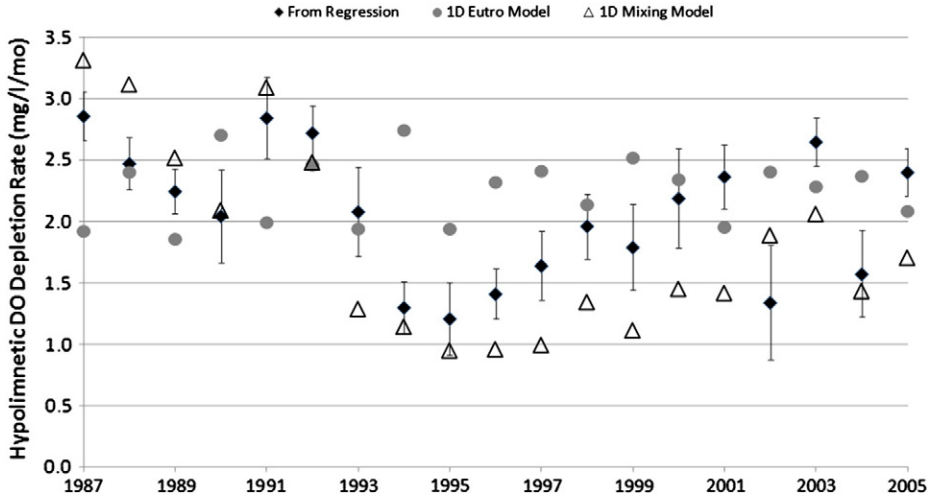

Fig. 8. Comparison of water column depletion rates from Rucinski et al. (2010) (open diamonds), linear regression (black diamonds; standard error shown in vertical error bars), and the model described here (solid circles).

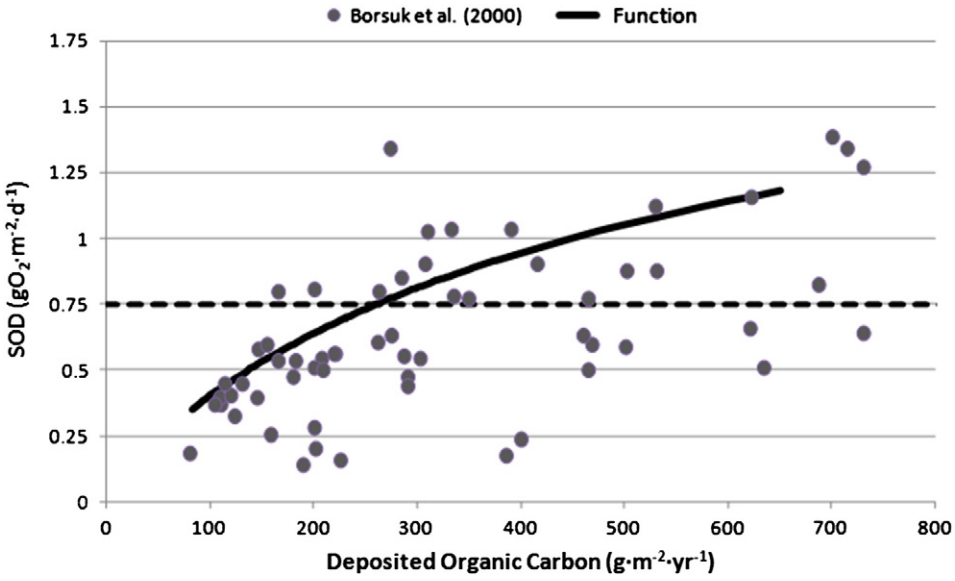

Fig. 9. Comparison of model calculated SOD (sediment oxygen demand) and sampled estuaries in Borsuk et al. (2001). Average of published Lake Erie SOD values is shown as dashed line. Solid line shows the obtained function relating SOD to deposited carbon. Solid circles show the values published in Borsuk et al. (2001).

between load and carbon deposition and then, by way of the modified Borsuk equation, created a TP–SOD relationship (Fig. 10):

$$\mathrm{SOD} = \left(\frac{SOD_{\max}\ TP_{load}}{K_{SOD} + TP_{load}}\right)$$

where $SOD_{\max}$ is the maximum sediment oxygen demand, TP_{load} is the annual total phosphorus load, and K_{SOD} represents a half-saturation constant. This approximation assumes that SOD reaches a new steady state with nutrient loading. The values for $SOD_{\max}$ and K_{SOD}, obtained by regression, are 0.98 g m^{-2} day^{-1} and 3847 tons/year, respectively. With this ability to adjust SOD based on loads, the model was used to investigate the response of several water quality metrics as a function of load and inter-annual variability in physical drivers.

To explore the system's response to altered loads and inter-annual variability in physical drivers, response curves were generated by scaling the 1997 seasonal load time-series by factors ranging between 0.1 and 2.0 and running the model with temperature and mixing patterns from each of the 19 years to generate response envelopes represented by the mean and standard deviation of the 19 cases. In each of these load scaling runs, we applied the same state variable initial conditions, representing observations from 1997. This approach allows development of response curves for the central tendency in hypoxic response and also emphasizes that the meteorological conditions in a given year can produce substantial deviation from that mean. So, while we can estimate the projected impact of a load reduction on average, the actual hypoxia metric might deviate substantially in any given year. The 1997 seasonal loading time series was used as the base case because it resulted in a steady state SOD equal to the observed rates and it represented loads and hypoxic extent typical of the recent era.

To compare the impacts of inter-annual variability in hydrometeorology with inter-annual variability in the seasonality of the loads, we ran the model with all 19 sets of actual seasonal loads for each of the

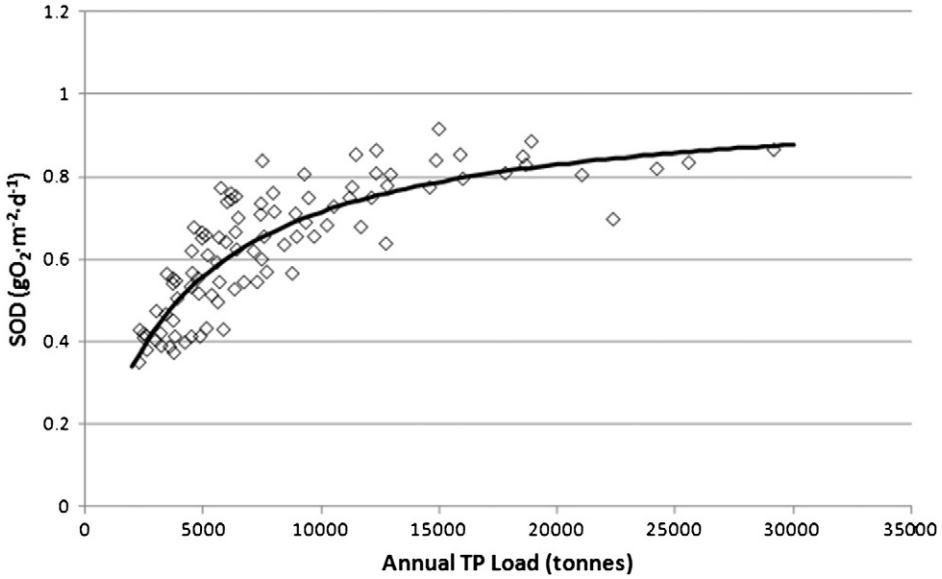

Fig. 10. Relationship between annual total phosphorus load and model calculated SOD. Model estimated values shown as open diamonds. Regression curve shown as solid line.

Table 4
Results of ANOVA testing the relative influence of interannual variability in hydrometeorology and load seasonality.

ANOVA						
Source of variation	SS	df	MS	F	P-value	F crit
Thermal regime	943.7686	18	52.43159	1753.322	0	1.635776
Seasonality	172.2021	18	9.566782	319.915	0	1.635776
Error	9.688943	324	0.029904			
Total	1125.66	360				

19 hydrometeorological conditions and used two-way ANOVA without replication to explore the relative contributions to overall variance. The results showed that variability in hydrothermal regime contributes 5 times more variance than does load seasonality (Table 4).

Response curves were generated for hypoxic area, hypoxic days, oxygen depletion rate, and bottom DO concentration as a function of annual TP load (Fig. 11) and DRP load (Fig. 12). It should be noted that the loads used in these curves represent total western and central basin loads, representing roughly 90% and 92% of the total TP and DRP loads, respectively. Eastern basin loads are assumed to not influence the central basin significantly. Observed means and standard deviations of these metrics, where available, are also plotted along with the model response to illustrate the model's ability to represent the general relationships, given the inherent variability in the observations, as well as capture the variability associated with inter-annual meteorology.

In a final model evaluation test, we also include (Fig. 11) observations from years considerably outside of the loading range in the 1987–2005 calibration/corroboration dataset. It shows the model's ability to capture most of those observations, including those with much higher loads from the 1960s and 1970s. This evaluation represents a more rigorous confirmation of the model beyond the corroboration using the 1987–2005 dataset, when P loads did not vary as much.

The response envelopes in Figs. 11 and 12 represent the influence of inter-annual variation in meteorology which can also be seen in the relationship between hypoxic area as a function of the average summer depth to the top of the hypolimnion (Fig. 13) where the error bars represent ±1 standard deviation for runs with the 19 different loads. These results are consistent with those of Lam et al. (1987), who showed that both loads and hydrothermal conditions contributed to hypoxic response from an earlier time period (1967–1982).

Discussion

This 1-dimensional linked hydrodynamic and eutrophication model was developed and corroborated to observations from 1987 to 2005, and verified with observations from the 1960s and 1970s. The model effectively captures both vertical and temporal trends in DO, as well as temporal trends in CHL, phosphorus, and zooplankton biomass and several key internal process rates. By incorporating a relationship between external load and SOD, the load–response curve envelopes, accounting for inter-annual variability in meteorological conditions, provide a valuable tool to reassess loading targets to Lake Erie with the goal of reducing hypoxia.

This analysis can be used to draw some management implications. By inspection of Fig. 11, it is clear that the western basin (WB) and central basin (CB) TP loads would have to be approximately 4300 MT/year (4804 MT/year total) to even reduce the hypoxic area to 2000 km^2, which is substantially lower than the current total load target of

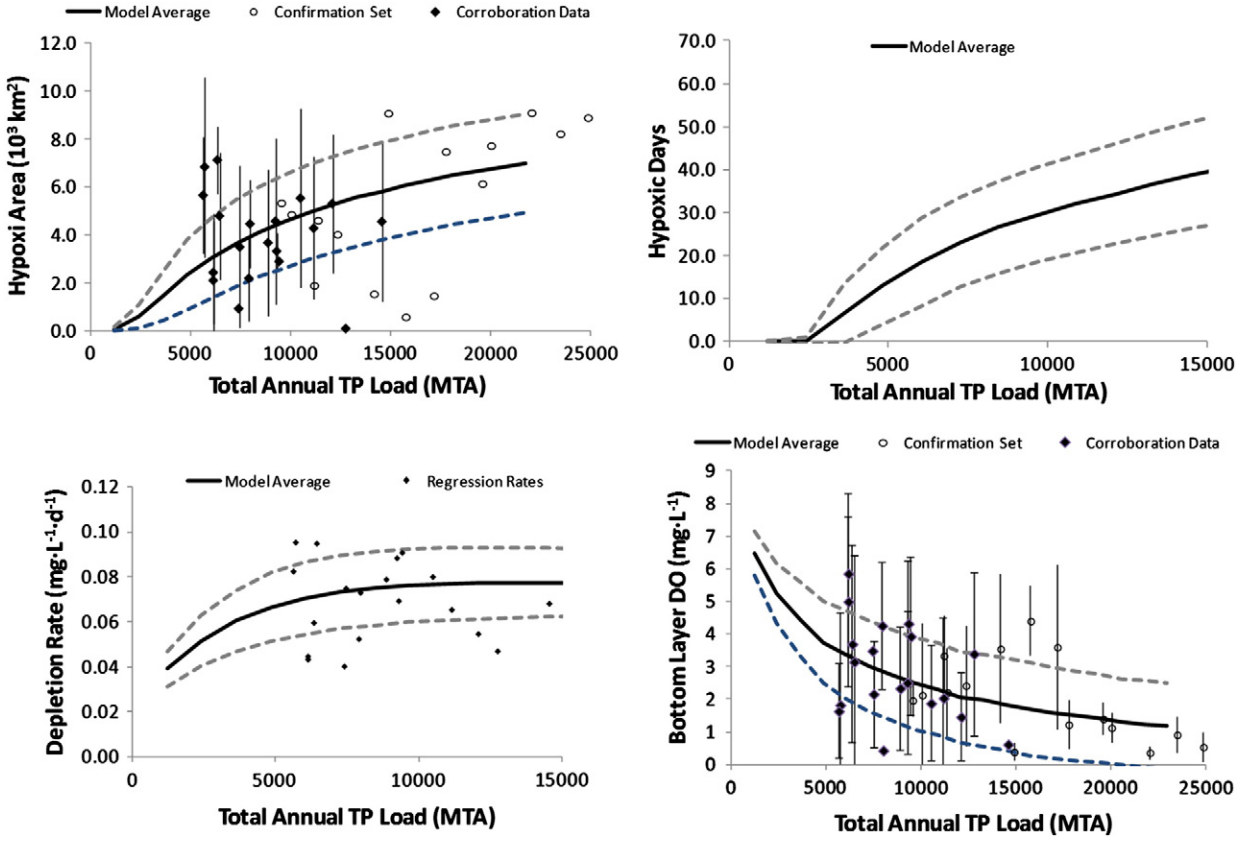

Fig. 11. Response of hypoxic area, hypoxic days, oxygen depletion rate, and bottom layer dissolved oxygen as a function of western and central basin TP loads. Curves represent the mean ± st. dev. of cases representing hydrometeorology from the years 1987–2005. Symbols and error bars are means and st. dev. of observations. Solid diamonds represent the 1987–2005 data sets. Open circle symbols are for years outside the 1987–2005 series.

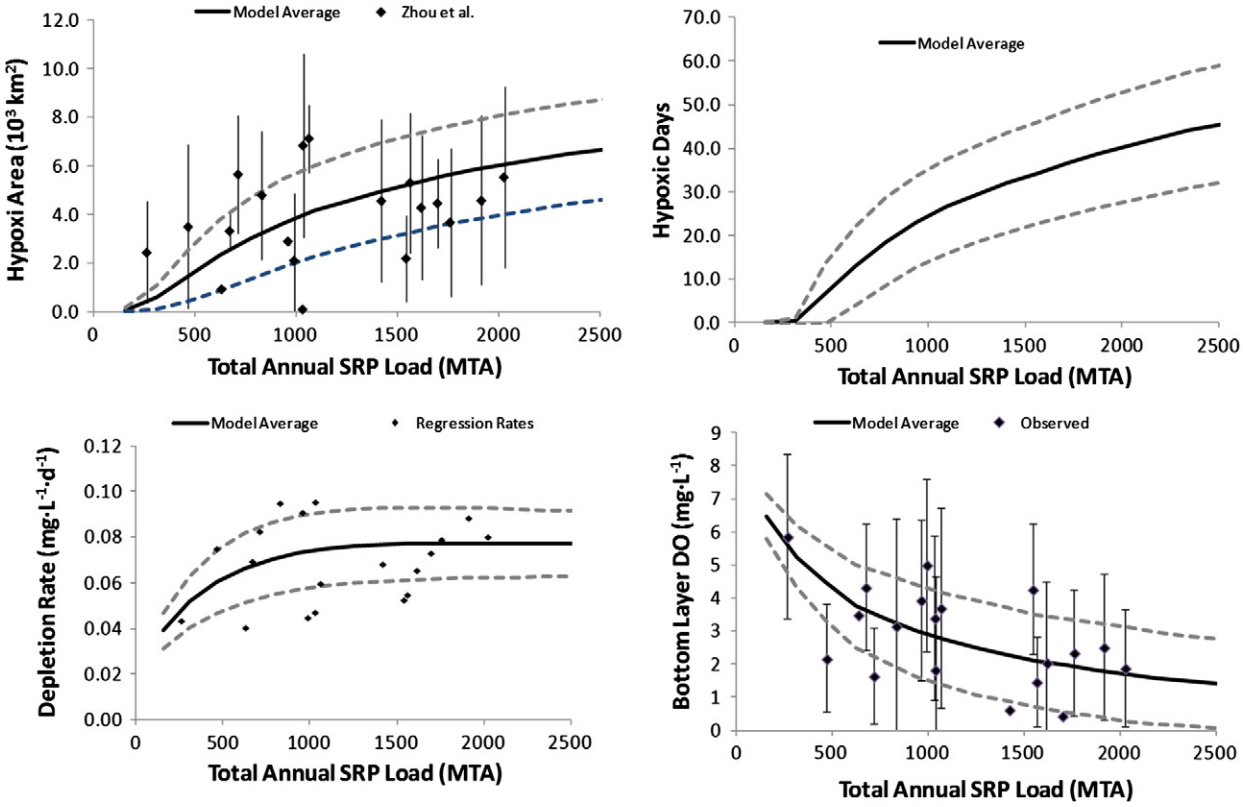

Fig. 12. Response of hypoxic area, hypoxic days, oxygen depletion rate, and bottom layer dissolved oxygen as a function of western and central basin DRP loads. Curves represent the mean ± st. dev. of cases representing hydrometeorology from the years 1987–2005. Symbols and error bars are means and st.dev. of observations. Solid diamonds represent 1987–2005 data sets.

11,000 MT. This is a 46% reduction from the 2003–2011 average loads and 56% below the current target. If a new target was developed for DRP (Fig. 12), achieving that hypoxic area would require a DRP load reduction to 550 MT/year (equivalent total load of 598 MT/year), a value roughly equivalent to values in the early 1990s. Because there has been such a significant increase in the DRP load since then, this represents a very substantial 78% reduction from the 2005–2011 average DRP load. It is important to note that these projections not only provide the central tendency in hypoxic response, but also include response envelopes that represent variation due to changes in meteorological conditions. That is, while it provides a hypoxia estimate based on a given load that would be expected on average, the actual hypoxia metric might deviate substantially in any given year.

It is also interesting to note that recent recommendations to reduce the occurrence of western basin cyanobacteria blooms may not be sufficient to significantly reduce central basin hypoxia. For example, the Ohio Lake Erie Phosphorus Task Force recommended that to keep blooms to acceptable levels, the March–June Maumee River TP loads (as a surrogate for all WB tributaries) should be less than 800 MT (Ohio EPA, 2013), which is a 31% reduction from the 2005–2011 average of 1160 MT (Richards, pers. com). If all western and central basin non-point sources were reduced by the same 31% and applied across

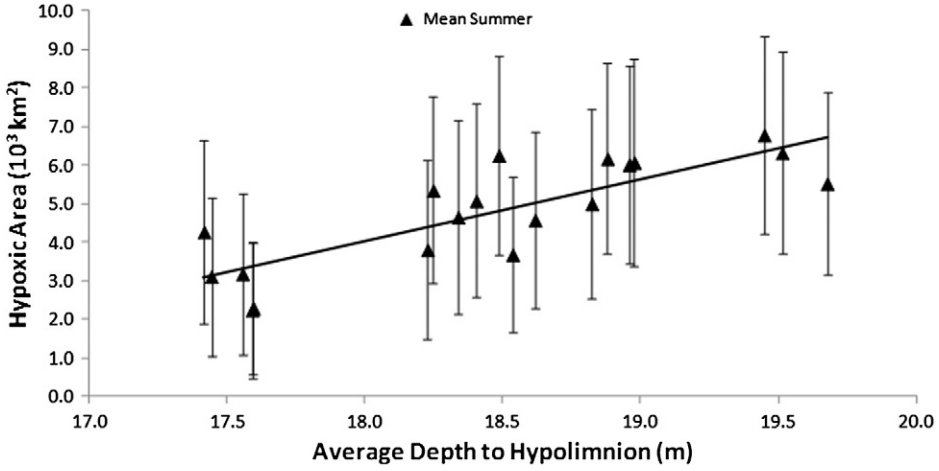

Fig. 13. Response of hypoxic area as a function of summer-average depth to the hypolimnion. Summer mean hypoxic area is shown in solid triangles and the uncertainty bars represent ± standard deviation of runs with loads from the 19 scenarios.

the full year, the resulting annual TP load would be reduced to 6273 MT/year, still considerably higher than the 4300 MT/year target identified above. So, in setting targets, it is important to recognize that western basin cyanobacteria and central basin hypoxia endpoints likely require separate considerations.

This analysis demonstrated the importance of both phosphorus loading and hydrometeorological stressors on hypoxia in the Central Basin of Lake Erie. Further, it demonstrated that inter-annual variability in the development and duration of summer thermal stratification could produce considerable variability in the hypoxic response for a given phosphorus load. Nevertheless, the findings for the relationship between hypoxic zone area and phosphorus loading has provided an excellent load reduction target to begin an adaptive management process aimed at minimizing the hypoxic zone to the greatest extent possible. To be sure, the model could be made more complex by adding processes (e.g., multiple phytoplankton functional groups, nitrification, and sediment diagenesis) and increasing dimensionality; however, those types of refinements should await the observation of the system response to the recommended phosphorus load reduction. Future work should investigate the potential effects of climate change on the response curves produced from this analysis.

Supplementary data to this article can be found online at http://dx.doi.org/10.1016/j.jglr.2014.02.003.

Acknowledgments

This research was supported in part by the NOAA Center for Sponsored Coastal Ocean Research grant NA07OAR432000 and the University of Michigan Graham Sustainability Institute. This paper is contribution no. 13-004 of the NOAA EcoFore-Lake Erie Project. The authors would like to thank Environment Canada: Water Science & Technology Branch, the EPA Great Lakes National Program Office, and NOAA-GLERL for sharing water quality data.

References

Anderson, T.R., 2005. Plankton functional type modelling: running before we can walk? J. Plankton Res. 27 (11), 1073–1081.
Beeton, A.M., 1963. Limnological survey of Lake Erie 1959 and 1960. Great Lakes Fisheries Commission Technical Report. No. 6.
Beletsky, D., Schwab, D.J., 2001. Modeling circulation and thermal structure in Lake Michigan: annual cycle and interannual variability. J. Geophys. Res. 106, 19745–19771.
Beletsky, D., Hawley, N., Rao, Y.R., Vanderploeg, H.A., Beletsky, R., Schwab, D.J., Ruberg, S.A., 2012. Summer thermal structure and anticyclonic circulation of Lake Erie. Geophys. Res. Lett. 39, L06605. http://dx.doi.org/10.1029/2012GL051002.
Beletsky, D., Hawley, N., Rao, Y.R., 2013. Modeling summer circulation and thermal structure of Lake Erie. J. Geophys. Res. Oceans 118. http://dx.doi.org/10.1002/2013JC008854.
Blumberg, A.F., Di Toro, D.M., 1990. Effects of climate warming on dissolved oxygen concentrations in Lake Erie. Trans. Am. Fish. Soc. 119, 210–223.
Blumberg, A.F., Mellor, G.L., 1987. A description of a three-dimensional coastal ocean circulation model. In: Heaps, N.S. (Ed.), Three-Dimensional Shelf Models, Coastal and Estuarine Sciences. American Geophys. Union, pp. 1–16.
Borsuk, M., Higdon, D., Stow, C., Reckhow, K., 2001. A Bayesian hierarchical model to predict benthic oxygen demand from organic matter loading in estuaries and coastal zones. Ecol. Model. 143, 165–181.
Bridgeman, T.B., Chaffin, J.D., Filbrun, J.E., 2013. A novel method for tracking western Lake Erie *Microcystis* blooms, 2002–2011. J. Great Lakes Res. 39 (1), 83–89.
Burns, N.M., Rockwell, D.M., Bertram, P.E., Dolan, D.M., Ciborowski, J.J.H., 2005. Trends in temperature, secchi depth, and dissolved oxygen depletion rates in the central basin of Lake Erie, 1983–2002. J. Great Lakes Res. 31, 35–49.
Charlton, M.N., Lean, D.R.S., 1987. Sedimentation, resuspension, and oxygen depletion in Lake Erie (1979). J. Great Lakes Res. 13 (4), 709–723.
Chen, C., Ji, R., Schwab, D.J., Beletsky, D., Fahnenstiel, G.L., Johengen, T.H., Vanderploeg, H.A., Eadie, B.J., Bundy, M., Gardner, W., Cotner, J., 2002. A model study of the coupled biological and physical dynamics in Lake Michigan. Ecol. Model. 152, 145–168.
Dolan, D.M., Chapra, S.C., 2012. Great Lakes total phosphorus revisited: 1. Loading analysis and update (1994–2008). J. Great Lakes Res. 38 (4), 730–740 (December).
Depew, D.C., Guildford, S.J., Smith, R.E.H., 2006. Nearshore–offshore comparison of chlorophyll a and phytoplankton production in the dreissenid-colonized eastern basin of Lake Erie. Can. J. Fish. Aquat. Sci. 63, 1115–1129.
DePinto, J.V., Young, T.C., McIlroy, M., 1986. Great Lakes water quality improvement: the strategy of phosphorus discharge control is evaluated. Environ. Sci. Technol. 20 (8), 752–759.
Di Toro, D.M., Thomas, N.A., Herdendorf, C.E., Winfield, R.P., Connolly, J.P., 1987. A post audit of a Lake Erie eutrophication model. J. Great Lakes Res. 13, 801–825.
Diaz, R.J., 2001. Overview of hypoxia around the world. J. Environ. Qual. 30, 275–281.
Di Toro, D.M., Connolly, J.P., 1980. Mathematical models of water quality in large lakes. Part 2: Lake Erie, EPA-600/3-80-065 Report, Duluth, MN.
Dolan, D.M., 1993. Point source loadings of phosphorus to Lake Erie: 1986–1990. J. Great Lakes Res. 19, 212–223.
Dolan, D.M., McGunagle, K.P., 2005. Lake Erie total phosphorus loading analysis and update: 1996–2002. J. Great Lakes Res. 31 (Suppl. 2), 11–22.
ECWSTB (Environment Canada, Water Science & Technology Branch), a. ftp://charon.cciw.ca (accessed June 2007).
El-Shaarawi, A.H., 1987. Water quality changes in Lake Erie, 1968–1980. J. Great Lakes Res. 13, 674–683.
Friedrichs, M.A.M., Hood, R.R., Wiggert, J.D., 2006. Ecosystem model complexity versus physical forcing: quantification of their relative impact with assimilated Arabian Sea data. Deep Sea Res. II 53, 576–600.
GLWQA, 1978. Great Lakes Water Quality Agreement.
IFYLE, 2006. NOAA Great Lakes Environmental Research Laboratory: International Field Years on Lake Erie (IFYLE). http://www.glerl.noaa.gov/ifyle/11/12/2006. GLNPO (Great Lake National Program Office) (http://cdx.epa.gov/ (accessed February 2007)).
Lam, D.C.L., Schertzer, W.M., Fraser, A.S., 1987. A post-audit analysis of the NWRI nine-box water quality model for Lake Erie. J. Great Lakes Res. 13, 782–800.
Leon, L.F., Smith, R.E.H., Hipsey, M.R., Bocainov, S.A., Higgins, S.N., Hecky, R.E., Antenucci, J.P., Guildford, S.J., 2011. Application of a 3D hydrodynamic-biological model for seasonal and spatial dynamics of water quality and phytoplankton in Lake Erie. J. Great Lakes Res. 37 (1), 41–53.
Lesht, B.M., Fontaine, T.D., Dolan, D.M., 1991. Great Lakes total phosphorus model: post audit and regionalized sensitivity analysis. J. Great Lakes Res. 17 (1), 3–17.
Matisoff, G., Neeson, T.M., 2005. Oxygen Concentration and Demand in Lake Erie Sediments. Journal of Great Lakes Research 31, 284–295.
Mellor, G.L., Yamada, T., 1982. Development of a turbulence closure model for geophysical fluid problems. Rev. Geophys. 20, 851–875.
Ostrom, N.E., Russ, M.E., Field, A., Piwinski, L., Twiss, M.R., Carrick, H.J., 2005a. Ratios of community respiration to photosynthesis and rates of primary production in Lake Erie via oxygen isotope techniques. J. Great Lakes Res. 31 (Supplement 2), 138–153.
Ostrom, N.E., Carrick, H.J., Twiss, M.R., Piwinski, L., 2005b. Evaluation of primary production in Lake Erie by multiple proxies. Oecologia 144, 115–124.
Rao, Y.R., Hawley, N., Charlton, M.N., Schertzer, W.M., 2008. Physical processes and hypoxia in the central basin of Lake Erie. Limnol. Oceanogr. 53, 2007–2020.
Redfield, A.C., 1934. On the proportions of organic derivations in sea water and their relation to the composition of plankton. In: Daniel, R.J. (Ed.), James Johnstone Memorial Volume, pp. 177–192.
Richards, R.P., 2006. Trends in sediment and nutrients in major Lake Erie tributaries, 1975–2004. Lake Erie Lakewide Management Plan 2006 Update, p. 22.
Richards, R.P., Baker, D.B., 2002. Trends in water quality in LEASEQ rivers and streams, 1975–1995. J. Environ. Qual. 31, 90–96.
Rosa, F., 1985. Sedimentation and sediment resuspension in Lake Ontario. J. Great Lakes Res. 11 (1), 13–25.
Rosa, F., Burns, N.M., 1987. Lake Erie central basin oxygen depletion changes from 1929–1980. J. Great Lakes Res. 13, 684–696.
Rucinski, Daniel K., Beletsky, D., DePinto, J.V., Schwab, D.J., Scavia, D., 2010. A simple 1-dimensional, climate based dissolved oxygen model for the central basin of Lake Erie. J. Great Lakes Res. 36, 465–476.
Schloesser, D.W., Stickle, R.G., Bridgeman, T.B., 2005. Potential oxygen demand of sediments from Lake Erie. J. Great Lakes Res. 31, 272–283.
Smith, D.A., Matisoff, G., 2008. Sediment oxygen demand in the central basin of Lake Erie. J. Great Lakes Res. 34 (4), 731–744.
Smith, R.E.H., Hiriart-Baer, V.P., Higgins, S.N., Guildford, S.J., Charlton, M.N., 2005. Planktonic primary production in the offshore waters of dreissenid-infested Lake Erie in 1997. J. Great Lakes Res. 31 (Supplement 2), 50–61.
Snodgrass, W.J., 1987. Analysis of models and measurements for sediment oxygen demand in Lake Erie. J. Great Lakes Res. 13, 738–756.
Snodgrass, W.J., Fay, L.A., 1987. Values of sediment oxygen demand measured in the central basin of Lake Erie, 1979. J. Great Lakes Res. 13, 724–730.
Twiss, M.R., McKay, R.M.L., Bourbonniere, R.A., Bullerjahn, G.S., Carrick, H.J., Smith, R.E.H., Winter, J.G., D'souza, N.A., Furey, P.C., Lashaway, A.R., Saxton, M.A., Wilhelm, S.W., 2013. Diatoms abound in ice-covered Lake Erie: an investigation of offshore winter limnology in Lake Erie over the period 2007 to 2010. J. Great Lakes Res. 38 (1), 18–30.
Wetzel, R.G., 2001. Limnology: Lake and River Ecosystems, 3rd edition. Academic Press 47.
Wool, T.A., Ambrose, R.B., Martin, J.L., Coormer, E.A., 2002. Water Quality Analysis Simulation Program (WASP). Version 6.0.
Woynarovich, E., 1961. The oxygen consumption of *Dreissena polymorpha* (Lamellibranchiate) at different temperatures. Ann. Biol. Tihany 28, 216.
Zhang, H., Culver, D.A., Boegman, L., 2008. A two-dimensional ecological model of Lake Erie: application to estimate dreissenid impacts on large lake plankton populations. Ecol. Model. 214, 219–241.
Zhou, Y., Obenour, D.R., Scavia, D., Johengen, T.H., Michalak, A.M., 2013. Spatial and temporal trends in Lake Erie hypoxia, 1987–2007. Environ. Sci. Technol. 47, 899–905.